

# Searching for Dark Absorption with Direct Detection Experiments

---

**Itay M. Bloch,<sup>a</sup> Rouven Essig,<sup>b</sup> Kohsaku Tobioka,<sup>a,c</sup> Tomer Volansky,<sup>a</sup> Tien-Tien Yu.<sup>b</sup>**

*Raymond and Beverly Sackler School of Physics and Astronomy, Tel-Aviv University, Tel-Aviv 69978, Israel*

<sup>a</sup>*Raymond and Beverly Sackler School of Physics and Astronomy, Tel-Aviv University, Tel-Aviv 69978, Israel*

<sup>b</sup>*C.N. Yang Institute for Theoretical Physics, Stony Brook University, Stony Brook, NY 11794-3800*

<sup>c</sup>*Department of Particle Physics and Astrophysics, Weizmann Institute of Science, Rehovot 7610001, Israel*

*E-mail:* [itaybloc@mail.tau.ac.il](mailto:itaybloc@mail.tau.ac.il), [rouven.essig@stonybrook.edu](mailto:rouven.essig@stonybrook.edu),  
[kohsakut@post.tau.ac.il](mailto:kohsakut@post.tau.ac.il), [tomerv@post.tau.ac.il](mailto:tomerv@post.tau.ac.il),  
[chiu-tien.yu@stonybrook.edu](mailto:chiu-tien.yu@stonybrook.edu)

**ABSTRACT:** We consider the absorption by bound electrons of dark matter in the form of dark photons and axion-like particles, as well as of dark photons from the Sun, in current and next-generation direct detection experiments. Experiments sensitive to electron recoils can detect such particles with masses between a few eV to more than 10 keV. For dark photon dark matter, we update a previous bound based on XENON10 data and derive new bounds based on data from XENON100 and CDMSlite. We find these experiments to disfavor previously allowed parameter space. Moreover, we derive sensitivity projections for SuperCDMS at SNOLAB for silicon and germanium targets, as well as for various possible experiments with scintillating targets (cesium iodide, sodium iodide, and gallium arsenide). The projected sensitivity can probe large new regions of parameter space. For axion-like particles, the same current direction detection data improves on previously known direct-detection constraints but does not bound new parameter space beyond known stellar cooling bounds. However, projected sensitivities of the upcoming SuperCDMS SNOLAB using germanium can go beyond these and even probe parameter space consistent with possible hints from the white dwarf luminosity function. We find similar results for dark photons from the sun. For all cases, direct-detection experiments can have unprecedented sensitivity to dark-sector particles.

---

## Contents

<b>1</b>	<b>Introduction</b>	<b>1</b>
<b>2</b>	<b>Axion-Like Particles</b>	<b>3</b>
2.1	ALPs as Dark Matter	4
2.2	ALPs from the Sun	4
<b>3</b>	<b>Dark photons</b>	<b>4</b>
3.1	Dark photons as Dark Matter	5
3.2	Dark photons from the Sun	5
<b>4</b>	<b>Analysis of Current and Future Experiments</b>	<b>6</b>
4.1	Signal Region	7
4.2	Current Experiments	7
4.3	Future Experiments	9
<b>5</b>	<b>Results</b>	<b>11</b>
<b>A</b>	<b>Rates for ALPs and dark photons in various materials</b>	<b>13</b>
<b>B</b>	<b>Solar <math>A'</math> Production</b>	<b>13</b>

---

## 1 Introduction

Significant experimental evidence and theoretical considerations suggest that the Standard Model (SM) of particle physics is incomplete. In particular, there is compelling evidence for the existence of dark matter (DM). Determining the identity of the DM particle is one of the most important problems in particle physics today.

Many DM candidates exist, with Weakly Interacting Massive Particles (WIMPs) being the most studied. Numerous direct-detection experiments probe for the elastic scattering of WIMPs (and other DM candidates) off ordinary matter [1]. However, it is entirely plausible that DM is composed of a (pseudo)scalar or a vector boson that can be *absorbed* in a material, thereby depositing its full kinetic and rest-mass energy. DM in the form of axions, axion-like particles (ALPs), and dark photons can have this property, see e.g. [2]. This paper focuses on the search of such DM candidates with existing and upcoming direct-detection experiments. For other types of searches see e.g. [3–13].

The axion was originally introduced as a solution to the strong CP problem [14, 15]. This pseudoscalar may couple in a model-dependent manner to the SM axial current,  $\partial^\mu a J_\mu^A / f_a$ , where  $f_a$  is the axion decay constant and indicates the scale at which the Peccei-Quinn [16] symmetry is broken. More generally, the spontaneous breaking of any

global symmetry combined with a small explicit breaking can lead to low-mass ALPs with a similar interaction. This interaction allows the axion or ALP to be absorbed in a target material, rather than scattering off it. The case of absorption in bound electrons, known as the axioelectric effect, has been originally suggested in [17, 18]. Numerous direct-detection experiments have conducted searches assuming that the ALP constitutes the galactic DM or is produced in the Sun, including CoGeNT [19], CDMS [20], EDELWEISS [21], XENON100 [22], and KIMS [23]. Here we show that other existing data can improve on these bounds and provide projections for future experiments. We find that future experiments could go beyond the strong stellar constraints.

Another simple DM candidate, present in many extensions of the SM, is the dark photon, which we denote as  $A'$ . The  $A'$  is a massive vector boson that can couple weakly to ordinary matter through kinetic mixing [24–28]. Significant ongoing experimental effort searches for an  $A'$ , see e.g. [29–31]. An intriguing possibility, however, is that the  $A'$  itself is sufficiently stable to play the role of the DM particle [32–34]. In this case, relic  $A'$ s may be absorbed by ordinary matter in direct-detection experiments, just like an ALP. Initial studies of this possibility were presented in [35]. We derive new direct-detection bounds that are more constraining than existing limits, and provide projected sensitivities.

We focus on the sensitivity gain achieved when lowering the threshold of direct-detection experiments. Traditionally, these experiments have been optimized to probe WIMPs with masses above  $\mathcal{O}(\text{GeV})$ , requiring sensitivity to nuclear recoil energies above  $\mathcal{O}(\text{keV})$ . However, many viable DM candidates have masses well below the GeV-scale, which can only be probed with new techniques [36]. DM scattering off electrons is one such technique suggested in [36]. Not only does this probe sub-GeV DM scattering, but a lower ionization threshold translates directly into a lower mass threshold for absorbing (nonrelativistic) DM.

XENON10’s sensitivity to single electrons [37] allows them to probe the lowest electron recoil energies, but without distinguishing signal from background events. This data was used to place a constraint on DM as light as a few MeV scattering off electrons [38] and on  $A'$  DM as light as the xenon ionization energy of 12.1 eV [35]. We revisit the latter limit below. More recently, the XENON100 experiment published a search for events with four or more electrons [39]. We show that this data improves constraints on sub-keV ALPs and  $A'$  DM. We also show that a CDMSlite dataset sensitive to  $\mathcal{O}(20)$  electrons [40] sets the strongest constraints for some  $A'$  DM masses.

Future experiments are expected to achieve improved sensitivity to even lower DM masses by lowering the threshold down to  $\mathcal{O}(\text{eV})$  and having a reduced background. A key to this improvement is the use of semiconductors or scintillators, which have band gaps of  $\mathcal{O}(\text{few eV})$ . The sensitivity gained by developing ultra-sensitive detectors able to probe one or a few electrons in semiconductors (e.g. SuperCDMS [40], DAMIC [41, 42]), scintillators, or two-dimensional targets has been studied in the context of sub-GeV DM scattering in [36, 43–47]. Below we study the prospects of such experiments to detect or constrain ALPs and  $A'$ s. Superconducting targets may probe even lower masses, either by DM scattering [48, 49] or DM absorption [50], in the future. Moreover, while beyond the scope of this paper, chemical-bond breaking could be used to probe nuclear recoils down

to 10 MeV [51, 52], while superfluid helium could probe nuclear recoils down to keV [53]. These would probe different couplings from the models considered here.

Finally, axions, ALPs, and dark photons may exist without constituting a significant fraction of the DM energy density. If sufficiently light, they would be produced in the Sun and can again be absorbed in direct-detection experiments. We will discuss constraints from existing experiments and provide projections for upcoming experiments. Since ALPs are dominantly produced in the Sun with  $\sim$ keV energies, no gain is achieved by experiments lowering their threshold. Instead, we focus on dark photons, which are produced also at low energies, so that lower thresholds could potentially probe beyond existing constraints.

## 2 Axion-Like Particles

The original “QCD” axion has a strict relation between its mass,  $m_a$ , and decay constant,  $f_a$ . More generally, however, ALPs may be described by independent  $m_a$  and  $f_a$ . Moreover, ALPs have model-dependent coupling to gluons, photons, and SM fermions. We are interested here in possible interactions with electrons, defined minimally by

$$\mathcal{L}_a = \frac{1}{2} \partial_\mu a \partial^\mu a - \frac{1}{2} m_a^2 a^2 + i g_{aee} a \bar{e} \gamma_5 e. \quad (2.1)$$

In the absence of additional couplings, the model dependence in  $g_{aee}$  can be absorbed in  $f_a$  and the two are related by  $g_{aee} = 2m_e/f_a$ . We show existing bounds and projections in the  $g_{aee}$  versus  $m_a$  parameter space.

The ALP interaction with electrons is responsible for the “axioelectric” effect [2, 17, 18, 54]. In analogy to the photoelectric effect, axions may be absorbed by bound electrons, ionizing them. Direct detection experiments search, in part, for ionized electrons and therefore offer an opportunity to search for ALPs via their coupling to electrons.

The ALP absorption cross section,  $\sigma_{\text{AE}}$ , may be related to the photoelectric absorption cross section,  $\sigma_{\text{PE}}$ , as

$$\sigma_{\text{AE}}(E) v_a \simeq \sigma_{\text{PE}}(E) \frac{3}{4} \frac{g_{aee}^2}{4\pi\alpha_{\text{EM}}} \frac{E^2}{m_e^2} \left( 1 - \frac{1}{3} v_a^{2/3} \right), \quad (2.2)$$

where  $E$  and  $v_a$  are the ALP’s energy and velocity, respectively [2, 17, 18]. We infer that the rate of absorption of non-relativistic ALP DM on an electron ( $n_a \sigma_{\text{AE}} v_a$ , where  $n_a$  is the ALP number density) has negligible dependence on  $v_a$ . The absorption spectrum is thus very narrow, helping to differentiate signal from background.

We take  $\sigma_{\text{PE}}(E)$  from Henke et al. [55, 56] and the *Handbook of Optical Constants of Solids* [57–60]. Discrepancies of  $\mathcal{O}(50\%)$  exist between different theoretical predictions for  $\sigma_{\text{PE}}(E)$  below  $\sim 300$  eV. The main sources of theory uncertainties arise from approximating the correlation between different electrons. We use the Henke calculations, which are favored by experimental data [61], for energies above 30 eV. Below 30 eV, we use the measurements compiled in [57–60].

## 2.1 ALPs as Dark Matter

Axions and ALPs may play the role of DM. The QCD axion is produced either thermally or through the misalignment mechanism and the decay of cosmological defects (for a review see e.g. [62, 63]). By tuning initial conditions or through late-time entropy dumping, axion DM has masses  $\lesssim 20 \mu\text{eV}$ . Non-thermal production through defects may allow for heavier axions; quite generally though, its mass must be  $\lesssim \text{eV}$  for it to be cold DM. Hot axions also require masses  $\lesssim \text{eV}$ .

ALPs could obtain the correct relic density in a wider mass range, via the misalignment mechanism, or by thermal or non-thermal production. It is thus interesting to constrain ALPs without assuming a specific production mechanism. The ALP absorption rate on electrons is

$$R_{\text{ALPs}} = 1.9 \times 10^{19} \text{ kg}^{-1} \text{ day}^{-1} \frac{g_{aee}^2}{A} \left( \frac{m_a}{\text{keV}} \right) \left( \frac{\sigma_{\text{PE}}}{\text{bn}} \right), \quad (2.3)$$

for a local DM energy density of  $\rho_{\text{DM}} = 0.4 \text{ GeV}/\text{cm}^3$ .

## 2.2 ALPs from the Sun

Independent of their relic density, ALPs may be produced in the Sun. The flux has been calculated in [64] and is largest at  $\mathcal{O}(\text{keV})$  energies.

Solar ALPs can be detected in direct-detection experiments [17, 18]. Limits on  $g_{aee}$  versus the ALP mass have been published by several direct detection experiments, among the strongest of which is the XENON100 collaboration analysis that used an S1 (primary scintillation) trigger with a 2 keV threshold [22]. The more recent S2-only analysis [39], which searched for events with only an ionization (S2) signal, has a much lower experimental threshold. However, given the drop in the solar ALP flux at low energies, as well as the sizable S2-only dataset, we checked that the S2-only analysis places weaker limits than found by [22]. Future xenon-based experiments can improve on these limits due to their large exposures and low expected backgrounds (see e.g. [65], although exposures  $\gtrsim 100$  ton-years are required to probe beyond white-dwarf cooling limits). Conversely, lowering the experimental threshold without a significant gain in exposure over XENON100 [22] only provides a negligible increase in sensitivity due to the rapidly falling solar flux below  $\mathcal{O}(\text{keV})$  energies. Since this paper is focused on discussing the potential gain from low-threshold experiments, we do not present the solar ALP limits.

## 3 Dark photons

The  $A'$  is a hypothetical massive vector boson of a broken (dark) gauge group  $U(1)_D$  that may kinetically mix with the SM hypercharge [24, 25]. At low energies, this mixing is dominantly between the  $A'$  and the SM photon. The relevant interactions are

$$\mathcal{L} \supset -\frac{1}{4} F'^{\mu\nu} F'_{\mu\nu} - \frac{\epsilon}{2} F^{\mu\nu} F'_{\mu\nu} + \frac{1}{2} m_{A'}^2 A'^\mu A'_\mu, \quad (3.1)$$

where  $\epsilon$  is the kinetic-mixing parameter,  $m_{A'}$  is the  $A'$  mass, and  $F^{\mu\nu}$  is the SM photon field strength. The mass  $m_{A'}$  can have two origins: a Stückelberg mass, which predicts

no additional degrees of freedom, or a Higgs mechanism, where the  $U(1)_D$  is broken spontaneously by an extra Higgs field. This distinction is irrelevant for  $A'$  DM detection, but important for detecting  $A'$  from the Sun. For the latter, we only consider a Stückelberg mass.

### 3.1 Dark photons as Dark Matter

For sufficiently small  $\epsilon$  and  $m_{A'}$  below twice the electron mass, the  $A'$  decay lifetime can be longer than the age of the Universe, allowing for the  $A'$  to constitute all the DM. Various production mechanisms exist, see e.g. [32–34]. The absorption of  $A'$  DM can be modeled as the absorption of a massive non-relativistic particle with coupling  $e\epsilon$  to electrons. We can then write the  $A'$  absorption cross-section in terms of  $\sigma_{\text{PE}}$ ,

$$\sigma_{A'}(E_{A'} = m_{A'}) v_{A'} \simeq \epsilon^2 \sigma_{\text{PE}}(E = m_{A'}), \quad (3.2)$$

where  $v_{A'}$  is the dark photon velocity [2]. The resulting absorption rate is given by (for  $\rho_{\text{DM}} = 0.4 \text{ GeV/cm}^3$ )

$$\text{Rate per atom} \simeq \frac{\rho_{\text{DM}}}{m_{A'}} \times \epsilon^2 \sigma_{\text{PE}}(E = m_{A'}). \quad (3.3)$$

We include in-medium effects. These are especially important for the detection of solar  $A'$ s, so we discuss them in the next subsection. For  $A'$  DM, the absorption rates are affected only by  $\lesssim 10\%$  for  $m_{A'} \gtrsim 100 \text{ eV}$ , although for  $m_{A'} \lesssim 100 \text{ eV}$ , the rate for xenon (germanium, silicon) is changed by a factor of  $\sim 0.2$ – $2.0$  ( $1.0$ – $1.15$ ,  $1.0$ – $1.8$ ).

### 3.2 Dark photons from the Sun

Direct detection experiments are sensitive to  $A'$ s from the Sun [66, 67]. The detection of these solar  $A'$ s is analogous to that of  $A'$  DM, but here the in-medium effects of the  $A'$  in the Sun may significantly affect production and detection. We focus on the Stückelberg case, and summarize the effect as described in [66, 68].

The matrix element for  $A'$  absorption in a medium is

$$\mathcal{M}(A'_{T,L} + i \rightarrow f) = -\frac{\epsilon m_{A'}^2}{m_{A'}^2 - \Pi_{T,L}} [e J_{\text{em}}^\mu]_{fi} \epsilon_\mu^{T,L}. \quad (3.4)$$

Here  $i$  and  $f$  denote the initial and final electron state and  $\Pi_{T,L}$  are the transverse (T) and longitudinal (L) in-medium polarization functions defined by

$$e^2 \langle J_{\text{em}}^\mu, J_{\text{em}}^\nu \rangle = \Pi_T \epsilon_i^{T\mu} \epsilon_i^{T\nu} + \Pi_L \epsilon_i^{L\mu} \epsilon_i^{L\nu}, \quad (3.5)$$

which encode the correlation function inside the medium. The absorption rate of the transverse and longitudinal modes of a solar  $A'$  in the detector frame is

$$\Gamma_{T,L}^{\text{detect}} = \frac{\epsilon_{T,L}^2 \text{Im } \Pi_{T,L}}{\omega}, \quad (3.6)$$

where the effective mixing angle is

$$\epsilon_{T,L}^2 = \frac{\epsilon^2 m_{A'}^4}{(m_{A'}^2 - \text{Re } \Pi_{T,L})^2 + (\text{Im } \Pi_{T,L})^2}. \quad (3.7)$$

For an isotropic and non-magnetic material with a refractive index  $n_{\text{refr}}$ , one has

$$\Pi_T = \omega^2(1 - n_{\text{refr}}^2), \quad \Pi_L = (\omega^2 - |\vec{q}|^2)(1 - n_{\text{refr}}^2), \quad (3.8)$$

where  $q = (\omega, \vec{q})$  is the  $A'$  4-momentum, with

$$n_{\text{refr}} = 1 - \frac{r_0}{2\pi} \lambda^2 \sum_A n_A (f_1^A + i f_2^A). \quad (3.9)$$

Here  $n_A$  denotes the density of atoms of type  $A$ ,  $\lambda$  is the de Broglie wavelength, and  $r_0$  is the classical electron radius,  $e^2/(m_e c^2) = 2.82 \times 10^{-15}$  m. The atomic scattering factors  $f_{1,2}$  are given in [55, 56]. The database [56] has  $f_1$  above 30 eV and  $f_2$  above 10 eV. To obtain  $f_1^{\text{Xe}}$  for energies below 30 eV, we use  $\text{Re}[n_{\text{refr}}]$  in Fig. 3 of [35].

The flux of solar dark photons is given by

$$\frac{d\Phi_{T,L}}{d\omega} = \frac{1}{4\pi d_\odot^2} \int_0^{R_\odot} dr 4\pi r^2 \frac{d\Gamma_{T,L}^{\text{prod},V}}{d\omega dV}, \quad (3.10)$$

where  $d_\odot = 1$  AU is the Earth-Sun distance and  $R_\odot = 6.96 \times 10^8$  m is Sun's radius. We consider the resonant production of the transverse and longitudinal modes, which gives the dominant component of the flux. The spectrum of the total number of events is

$$\frac{dN_{\text{events}}}{d\omega} = VT \frac{\omega}{\sqrt{\omega^2 - m_{A'}^2}} \text{Br} \left( \frac{d\Phi_T}{d\omega} \Gamma_T^{\text{detect}} + \frac{d\Phi_L}{d\omega} \Gamma_L^{\text{detect}} \right), \quad (3.11)$$

where  $V, T$  are the detector's fiducial volume and exposure time, respectively. The ratio of the ionization rate to the absorption rate,  $\text{Br}$ , is unity for the energies of interest. The spectrum has a sharp rise at the mass threshold because of the resonant production of the longitudinal mode.

## 4 Analysis of Current and Future Experiments

In this section, we describe how we derive bounds on ALPs and  $A'$ s using existing data from XENON10 [37], XENON100 [39], and CDMSlite [40], and how we derive projections for possible future experiments.

The low-mass reach of an experiment for ALP DM or  $A'$  DM absorption depends on the type of material used as a target. Xenon-based targets have a low-mass reach of 12.1 eV, while semiconductor- or scintillator-based experiments have a band gap, which is lower by about an order of magnitude, allowing such experiments to lower sensitivity down to  $\sim$ eV DM masses.

## 4.1 Signal Region

To extract optimal limits, we need to take into account the spectral shape of the signal in the detector, which depends not only on the detector energy resolution. In particular, an electron that absorbs an ALP or  $A'$  (the ‘primary’ electron) is ionized and its resulting kinetic energy (total minus binding) is converted to ionizing additional (‘secondary’) electrons. The number of secondary electrons produced fluctuates from event to event. Their variance and average number can be predicted in a given experiment, either by modeling the secondary interactions or through measurements. For a highly energetic primary electron, this variance usually dominates over the detector resolution.

We estimate below, either directly from the experimental data or from theoretical expectations, the variance and detector resolution (adding them in quadrature if needed), and smear the theoretical spectrum accordingly. To derive a conservative limit, we choose a single bin containing 95% of the signal and demand that it is less than the data at 90% C.L.. For the solar  $A'$  signal, we use a slightly simpler procedure, since the signal is distributed over a wider energy range: we first calculate the energy range (from  $m_{A'}$  upwards) that contains 95% of the signal, then smear the first and last bins, and require the signal to be less than the data at 90% C.L. in the resulting (smeared) energy range. The energy range we can use is limited by the ionization threshold in xenon ( $> 12.1$  eV) and by the band gap for the other materials (see below Eq. (2.2)). Note that the atomic data for NaI does not below below 30 eV, and so we do not go below 30 eV.

## 4.2 Current Experiments

We consider the following existing datasets:

- **XENON10:** The XENON10 experiment uses xenon as the target material and presented results using 15 kg-days of data with an S2 (ionization signal) trigger threshold set to a single electron [37]. Previous work used these data to derive conservative bounds on sub-GeV DM [38], solar  $A'$  [66], and  $A'$  DM [35]. In the latter two, the signal was required to be less than the *total* number of observed S2 events with  $\leq 80$  electrons, without taking into account spectral information. Here we use the spectral information to place more stringent bounds, except near threshold ( $\sim 15 - 30$  eV), where the bound is in reality slightly weaker. We take the signal efficiency times acceptance to be 0.92 for events with  $\geq 2$  electrons. For single electrons, the efficiency is only about 0.5, and we require the signal event rate to be less than 23.4 events/kg/day [38].

The number of secondary ionization electrons is challenging to calculate precisely, but we model it as discussed in [38]. Each electron produces  $\sim 27.0 \pm 6.2$  photoelectrons (PE), which are the actual signal seen by the XENON10 detector and defines the detector resolution. In [37], the data has already been converted from the number of PEs to the number of electrons. In Fig. 1 (top), we reproduce the spectrum of events (orange histogram) shown in Fig. 2 of [37]. We also show (in blue) a hypothetical DM ALP/ $A'$  signal, with the normalization chosen at the 90% C.L. limit, at two different masses (100 eV and 1100 eV). The pink and magenta gaussian lines show the signal shape that produces the worst and best limit, respectively, for the same two DM masses when



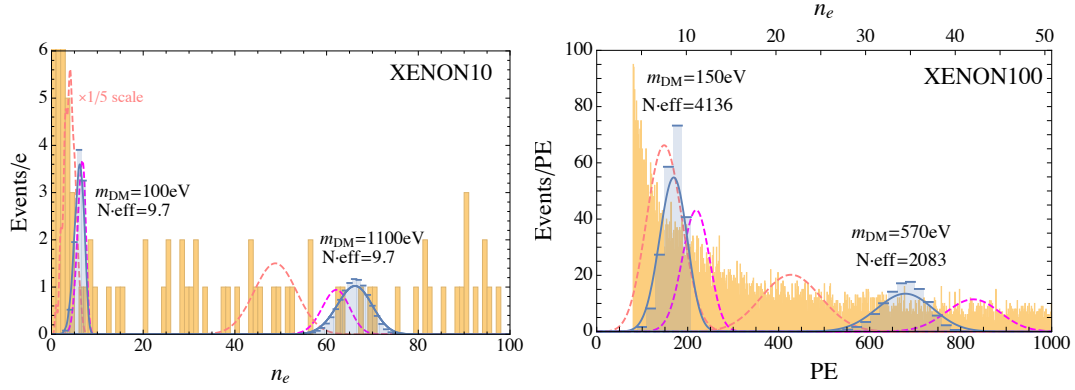


**Figure 1.** Ionization (S2-only) data from XENON10 [37] (left) and XENON100 [39] (right). Top plot shows the data as the number of observed electrons, while bottom plot shows the data as the number of photoelectrons (PE) on the bottom axis and the corresponding number of electrons ( $1e^- = 19.7PE$ ) on the top axis. Blue gaussian lines on each plot show two examples of the expected observed signal shape for two different DM (ALP or  $A'$ ) masses. The blue histogram shows the signal distribution in terms of the number of electrons produced in the detector. Varying the secondary ionization model produces different signal shapes and thus different limits. We show the signal shape in pink and magenta that produces, respectively, the worst and best limit for the same two DM masses when varying the secondary ionization model. Numbers next to the blue curves give the 90% C.L. upper bound times efficiency on the number of signal events for those masses.

varying the secondary ionization model. In Fig. 2, we show examples of solar  $A'$  spectra. Since the signal spans a wider energy range, the uncertainty in the secondary ionization modeling should be small, and we do not include the uncertainty.

- **XENON100:** The XENON100 collaboration presented S2-only data with events down to 80 PE, corresponding to about 4 electrons, in [39]. The data listing the number of PE for each event is reproduced in Fig. 1 (bottom), where we bin the data in 1 PE bins. The mean number of PE generated by one electron is  $19.7 \pm 0.3$ , with a width of  $6.9 \pm 0.3$  PE/electron [39]. Our signal calculation includes the acceptance and trigger efficiencies from [39]. As for XENON10 above, we show a hypothetical DM ALP/ $A'$  signal in blue at two different masses (150 eV and 570 eV). The pink and magenta gaussian lines again show, for the same two DM masses, the signal shape that produces the worst and best limit when varying the secondary ionization model. We derive the bound on solar  $A'$ s as discussed above. The bound on sub-GeV DM scattering off electrons based on this data will be presented in [69].
- **CDMSlite:** The SuperCDMS collaboration reported results with a threshold of 56 eV from a low-threshold “CDMSlite” run in [40]. To derive a bound, we take the data from Fig. 3 of [40] and apply all efficiencies and cuts (note that Fig. 3 is not corrected for the trigger efficiency). We treat the energy range 56 eV–140 eV as a single bin, taking the data from Table I. The total resolution of the signal (combining the experimental resolution and fluctuations in the number of secondary electrons) can be inferred from

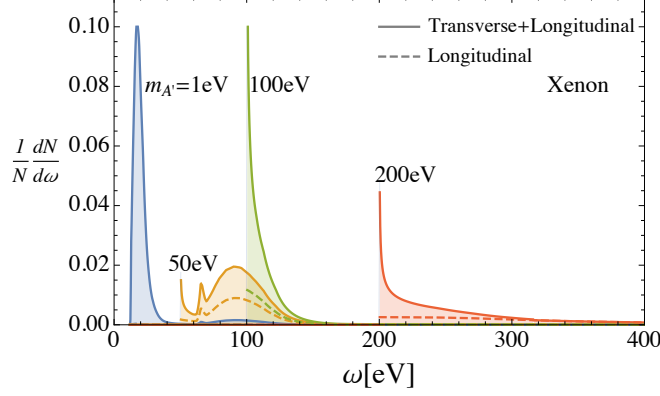


**Figure 2.** The normalized spectra of the total number of events for dark photons ( $A'$ ) from the Sun in a xenon detector. The combined transverse and longitudinal modes (**solid**) and the longitudinal mode alone (**dashed**) are shown for  $m_{A'} = 1, 50, 100$ , and  $200$  eV. The spectrum of the  $m_{A'} = 1$  eV case is cut off by the xenon ionization energy,  $12.1$  eV.

the observed electron capture peaks. Thus we adopt  $\sigma = 18.24$  eV ( $30.68$  eV,  $101$  eV) for the mass ranges  $[56$  eV,  $160$  eV] ( $[160$  eV,  $1.3$  keV],  $[1.3$  keV,  $10.37$  keV]).

### 4.3 Future Experiments

Future experiments are expected to have lower thresholds, allowing them to probe lower DM masses. To derive projections, we take into account expected physics backgrounds, but assume zero detector dark counts, i.e. no spontaneous creation of electron-hole pairs that mimic a signal.

- **SuperCDMS SNOLAB HV Ge and Si:** The next-generation SuperCDMS experiment will be deployed at SNOLAB. A high-voltage (HV) version will attempt to use a large bias voltage to achieve the same Luke-Neganov-phonons amplification of an ionization signal as the previous CDMSlite versions. Ultra-sensitive phonon detectors may achieve sensitivity down to single electrons, allowing the threshold to be given by the band gap ( $0.67$  eV for Ge,  $1.1$  eV for Si). The projected exposures are  $20$  ( $10$ ) kg-years for germanium (silicon) [1]. Our projections assume the following backgrounds:

- **Germanium:** We use a preliminary estimate by the SuperCDMS collaboration in [70]. This estimate includes backgrounds from tritium  $\beta$ -decay (a flat background on a log-log plot between  $\sim 1$  eV to a few keV), various x-ray lines produced by cosmogenic activation, and solar neutrinos (only relevant at energies  $\lesssim 10$  eV).

We assume that an electron in germanium absorbs a DM particle of mass  $m_{\text{DM}}$ , which must be larger than the band gap  $E_g$ . The kinetic energy ( $E_e - E_g = m_{\text{DM}} - E_g$ ) of this primary electron is converted into additional electron-hole pairs. The mean total number of electron-hole pairs created is

$$\langle Q(E_e) \rangle = 1 + \lfloor (E_e - E_g) / \varepsilon_e \rfloor, \quad (4.1)$$

where  $\varepsilon_e$  is the mean energy per electron-hole pair and  $\lfloor y \rfloor$  rounds  $y$  down to the nearest integer. Fluctuations around the mean are given by the Fano factor,  $F \equiv \sigma_Q^2 / \langle Q \rangle$ ,

Element	$\varepsilon_e$ [eV]	$E_g$ [eV]	$\sigma_{ee}$ at $E_e = 1$ keV [eV]
Ge	2.9	0.67	19.4
Si	3.6	1.1	21.7
NaI	17.7	5.9	47.8
CsI	19.2	6.4	50.0
GaAs	4.2	1.52	23.4

**Table 1.** Mean energy to create an electron-hole pair ( $\varepsilon_e$ ), band gap energy ( $E_g$ ), and signal width ( $\sigma_{ee}$ ) at ionization energies of 1 keV from Eq. (4.2) in various semiconductors (Si, Ge) and scintillators (NaI, CsI, GaAs).

where  $\sigma_Q^2$  is the variance. To calculate the width in the signal’s energy, we add in quadrature the energy resolution of the phonon detectors,  $\sigma_t$ , and the fluctuations in the number of secondary electron-hole pairs,

$$\sigma_{ee} = \varepsilon_e \sqrt{\frac{\sigma_t}{q_e V_b} + F \langle Q(E_e) \rangle}. \quad (4.2)$$

Here,  $V_b$  is the bias voltage, so one electron-hole pair will produce a total phonon energy of  $q_e V_b$ , where  $q_e = 1$  is the electron’s charge. For DM absorption, where  $E_e = m_{\text{DM}}$ , this equation becomes

$$\frac{\sigma_{ee}}{m_{\text{DM}}} \simeq \frac{\sqrt{\frac{\sigma_t}{q_e V_b} + F \langle Q(E_e) \rangle}}{\langle Q(E_e) \rangle - 1 + \frac{E_g}{\varepsilon_e}}. \quad (4.3)$$

For large enough  $Q$ , the signal shape is dominated by the Fano factor.

For germanium (and all other elements below), we take  $F = 0.13$  [72, 73]. While  $F$  varies less than 50% over almost two orders in magnitude in energy [72], measurements of  $F$  at energies below  $\sim 200$  eV would be desirable. We take  $\sigma_t = 10$  eV, although the precise value makes a difference only at the lowest masses above the band gap when only  $\mathcal{O}(\text{few})$  electrons are created. We set  $V_b = 100$  V, and use the values of  $\varepsilon_e$  and  $E_g$  for germanium (and other elements) in Table 1 [74, 75]. We list  $\sigma_{ee}(1 \text{ keV})$  as an example of the signal widths for various elements.

- **Silicon:** Silicon does not have the same low-energy x-ray lines produced by cosmogenic activation. However,  $^{32}\text{Si}$  is a relatively large contaminant and a low-energy  $\beta$ -emitter. Together with tritium, this produces a flat background at energies  $\lesssim 10$  keV, which we take to be 350 events/keVee/kg/year based on preliminary estimates by the SuperCDMS collaboration [76]. We take  $\sigma_t = 10$  eV, although the precise value is again only important just above the band gap. See Table 1 for the values of  $\varepsilon_e$ ,  $E_g$ , and  $\sigma_{ee}(1 \text{ keV})$  for silicon.<sup>1</sup>

<sup>1</sup>Future versions of the DAMIC experiments [42, 77], using so-called “Skipper CCDs”, could allow them to reduce their threshold to near the band gap of silicon [78]. The expected exposure is about 100 gram-years, less than the expected SuperCDMS exposure for silicon. Our projections for SuperCDMS can be rescaled easily to get projections for DAMIC.

- **Scintillators (NaI, CsI, and GaAs):** We show projections for hypothetical future experiments using scintillating targets with sensitivity down to one or more photons. Such experiments have been argued also to have great potential to sub-GeV DM scattering off electrons [47]. We make projections for three scintillating targets, sodium iodide, cesium iodide, and gallium arsenide, although other possibilities exist [47]. We assume a flat  $\beta$ -decay background of 350 events/keVee/kg/year as for the silicon projection above. We do not consider any x-ray lines activated by cosmogenics. We ignore the  $\sigma_t$  term in Eq. (4.2), and use the values listed in Table 1 (see also [47]).

## 5 Results

Existing constraints and projected sensitivities are shown for ALP ( $A'$ ) DM on the left (right) of Fig. 3. For ALPs, we see that the newly derived direct detection bounds from XENON100 and CDMSlite partially improve on published bounds from CoGeNT, CDMS, XENON100, EDELWEISS, and KIMS [19–23]. However, we see that these are weaker than stellar cooling bounds [35, 68, 79–83]. Prospective searches, especially SuperCDMS SNOLAB HV with germanium, could improve by a factor of a few beyond the stellar cooling constraints. Intriguingly, this includes probing part of the region consistent with a possible hint for anomalous energy loss in white dwarf stars [79, 83–85].

For  $A'$  DM, we have derived several constraints that go beyond the constraints from the anomalous energy loss in the Sun, horizontal-branch (HB) stars, and red-giant stars [35] (see also [66, 68, 81]). First, we have updated the bound derived in [35] based on the low-threshold XENON10 data [37]. We find that this bound disfavors a gap of several hundred eV in mass between the Sun and HB cooling bounds. Existing CDMSlite and XENON100 data disfavor additional parameter space beyond this. Prospective searches by SuperCDMS SNOLAB HV using germanium or silicon targets can probe up to more than an order of magnitude in  $\epsilon$  beyond existing constraints for sub-keV  $A'$  masses. New experiments using scintillator targets with sensitivity to one or a few photons can have similar reach.

We show the results for the solar  $A'$  in Fig. 4. We find that existing constraints from XENON10, XENON100, and CDMSlite are weaker than the stellar cooling constraints [68, 79–81]. We checked that data from KIMS [23], in the absence of a background model, provides a weaker bound (not shown) than CDMSlite. However, the future SuperCDMS, as well as possible scintillating target experiments, can significantly improve on existing bounds for  $A'$  masses below  $\sim 10$  eV.

Significant progress is being made in lowering the threshold of DM direct detection experiments. In this work, we studied the implications of this progress for searching for dark absorption. We find that planned and possible new experiments, using semiconducting and scintillating targets, can significantly improve on existing constraints, even probing well beyond astrophysical bounds. This provides unprecedented sensitivity to low-mass dark photons and ALPs.

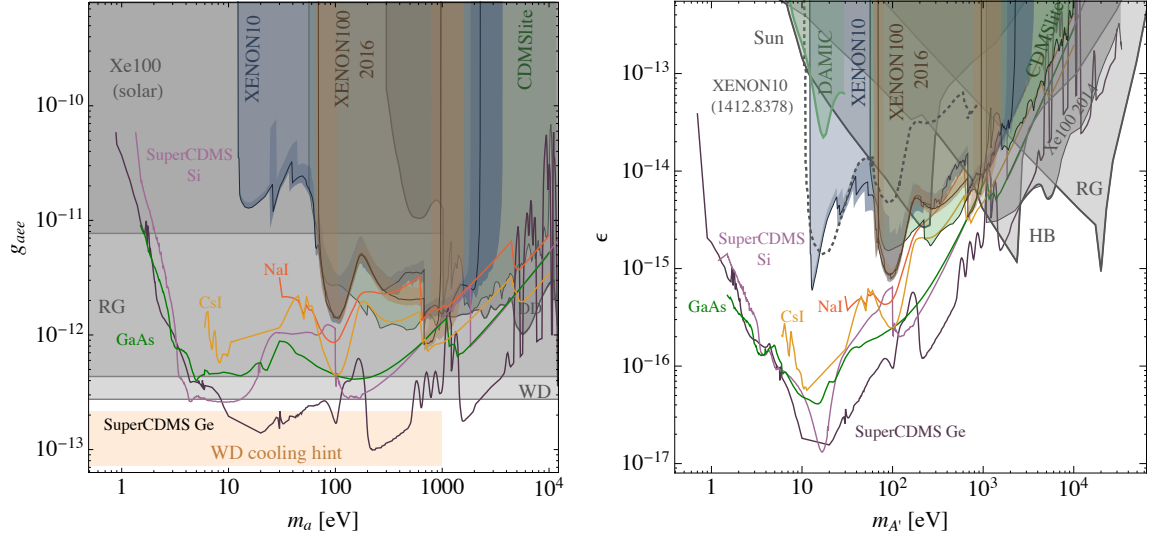


**Figure 3.** Constraints (shaded regions) and prospective sensitivities (solid colored lines) for axion-like particle (ALP) dark matter (left) and dark-photon ( $A'$ ) dark matter (right), assuming that the ALP/ $A'$  constitutes all the dark matter. **Colored regions** show constraints from XENON10, XENON100, and CDMSlite, as derived in this work, as well as the DAMIC results for  $A'$  from [71]. **Shaded bands** around XENON10 and XENON100 limits show how the bound varies when changing the modeling of the secondary ionization in xenon. **Deep- and light-purple solid lines** show projected 90% C.L. sensitivities for SuperCDMS SNOLAB HV using either Ge (20 kg-years) or Si (10 kg-years) targets, respectively. **Yellow, orange, and green solid lines** show projected sensitivities for hypothetical experiments with the scintillating targets CsI, NaI, and GaAs, assuming an exposure of 10 kg-years. All projections assume a realistic background model discussed in the text, but zero dark counts to achieve sensitivity to low-energy electron recoils. In-medium effects are included for all  $A'$  constraints and projections. Shaded gray regions show known constraints from anomalous cooling of the Sun, red giant stars (RG), white dwarf stars (WD), and/or horizontal branch stars (HB), which are independent of the ALP or  $A'$  relic density. Also shown (left) are the combined bounds from XENON100 [22], EDELWEISS [21], CDMS [20], and CoGeNT [19]; and (right) a bound derived in [35] based on XENON100 data from 2014 [22]. Shaded orange region in left plot is consistent with an ALP possibly explaining the white dwarf luminosity function.

### Note added:

While completing this work, we became aware of [86], which considers related topics.

### Acknowledgments

We thank Haipeng An, Ranny Budnik, Lauren Hsu, Maxim Pospelov, Josef Pradler, and Javier Redondo for useful discussions or correspondence. R.E. is supported by the DoE Early Career research program DESC0008061 and through a Sloan Foundation Research Fellowship. T.-T.Y. is also supported by grant DESC0008061. T.V. is supported by the European Research Council (ERC) under the EU Horizon 2020 Programme (ERC-CoG-

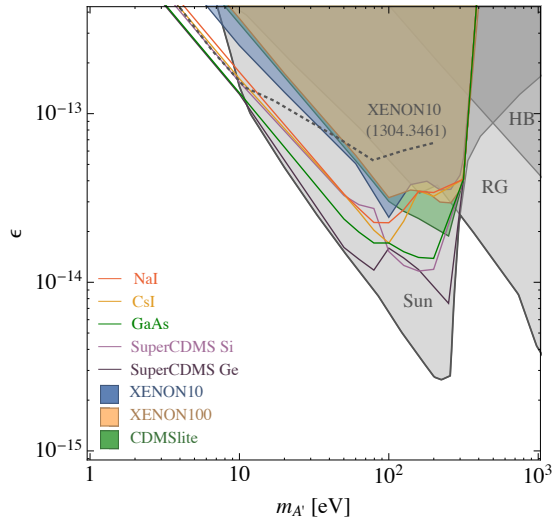


**Figure 4.** Constraints (shaded regions) and prospective sensitivities (solid colored lines) for dark-photons ( $A'$ ) with a Stückelberg mass from the Sun via resonant production (including in-medium effects). **Colored regions** show constraints from XENON10, XENON100, and CDMSlite, as derived in this work. **Deep- and light-purple solid lines** show projected 90% C.L. sensitivities for SuperCDMS SNOLAB HV using either Ge (20 kg-years) or Si (10 kg-years) targets, respectively. **Yellow, orange, and green solid lines** show projected sensitivities for hypothetical experiments with the scintillating targets CsI, NaI, and GaAs, assuming an exposure of 10 kg-years. All projections assume a realistic background model discussed in the text, but zero dark counts to achieve sensitivity to low-energy electron recoils. Shaded gray regions show constraint from anomalous cooling of the Sun. Also shown (dotted line) is the bound derived in [66] based on XENON10 data [22].

2015 - Proposal n. 682676 LDMThExp), by the PAZI foundation, by the German-Israeli Foundation (grant No. I-1283- 303.7/2014) and by the I-CORE Program of the Planning Budgeting Committee and the Israel Science Foundation (grant No. 1937/12).

## A Rates for ALPs and dark photons in various materials

In Fig. 5, we show the couplings  $\epsilon$  and  $g_{aee}$  for detecting 1 event/kg/year in a variety of materials for the  $A'$  and ALP models, respectively, as a function of mass. Note that these calculations do not depend on any background model. Therefore, one can easily translate these rates into a projection for a given background model or a limit for a given set of experimental data.

## B Solar $A'$ Production

A detailed description of the solar dark photon production and absorption rate can be found in Ref. [66]. We describe the relevant equations for the Stueckelberg case here.

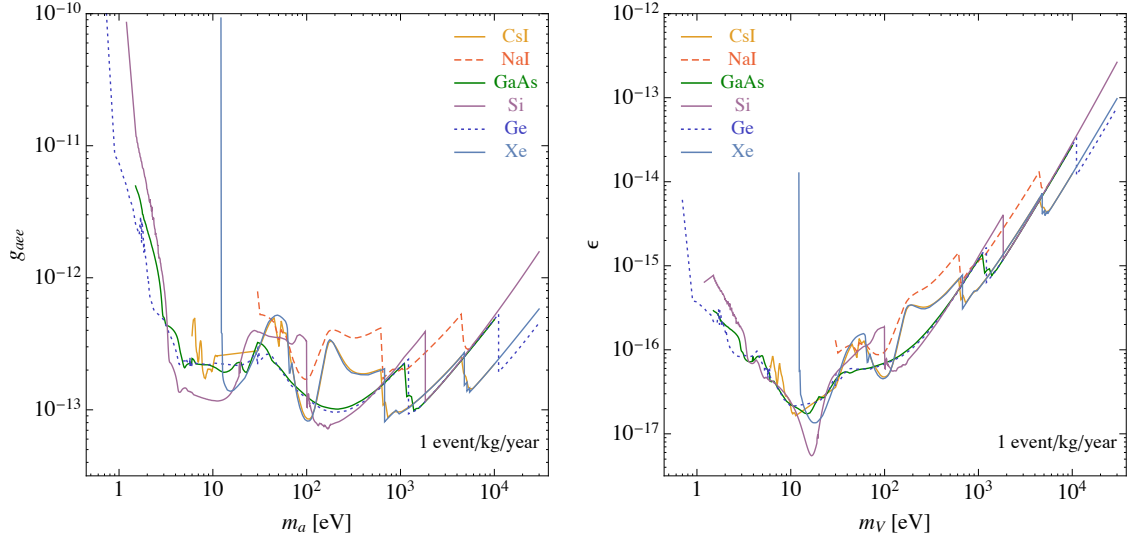


**Figure 5.** Couplings needed for 1 event/kg/year for ALPS (**left**) and  $A'$  (**right**). GaAs and Ge, and Xe and CsI have very similar behaviors due to similar refractive indices.

The production rate is given by

$$\frac{d\Gamma_{T,L}^{prod,V}}{d\omega dV} = \epsilon_{T,L}^2 \frac{d\Gamma_{T,L}^{prod}}{d\omega dV} \quad (\text{B.1})$$

where  $\epsilon_{T,L}$  is the effective mixing angle defined in Eq. (3.7). Inside the Sun the photon self energy is given by

$$\text{Re } \Pi_T = \omega_p^2, \quad \text{Re } \Pi_L = \omega_p^2(m_{A'}^2/\omega^2), \quad (\text{B.2})$$

$$\text{Im } \Pi_{T,L} = -\omega(1 - e^{-\omega/T})\Gamma_{T,L}^{abs}, \quad (\text{B.3})$$

where  $\omega_p(r) = e^2 n_e(r)/m_e$  is the plasma frequency inside the Sun,  $n_e$  is the electron density inside the Sun, and  $m_e$  is the electron mass [67]. There are two primary production modes for the dark photon: resonant production and bremsstrahlung.

For below the maximum plasma frequency  $\omega_p^{max} \simeq 300$  eV, the dominant contribution to the flux is longitudinal resonant production. The resonant production rate is given as

$$\left. \frac{d\Gamma_{T,L}^{prod,V}}{d\omega dV} \right|_{res} = \frac{\epsilon^2 m_{A'}^2 \sqrt{\omega^2 - m_{A'}^2}}{2\pi(1 - e^{\omega/T})} \delta(m_{A'}^2 - \text{Re } \Pi_{T,L}) \quad (\text{B.4})$$

Using Eq. (3.10), we obtain the corresponding flux from the resonant production,

$$\left. \frac{d\Phi_L}{d\omega} \right|_{res} = \frac{1}{4\pi d_\odot^2} \frac{\epsilon^2 m_{A'}^2 r^2(\omega_p) \omega^3}{e^{\omega/T(\omega_p)} - 1} \left. \frac{2}{d\omega_p^2/dr} \right|_{\omega_p=\omega} \quad (\text{B.5})$$

$$\left. \frac{d\Phi_T}{d\omega} \right|_{res} = \frac{\epsilon^2}{4\pi d_\odot^2} \frac{m_{A'}^4 r^2(\omega_p) \sqrt{\omega^2 - m_{A'}^2}}{e^{\omega/T(\omega_p)} - 1} \left. \frac{2}{d\omega_p^2/dr} \right|_{\omega_p=m_{A'}}. \quad (\text{B.6})$$

For  $\omega > \omega_p^{max}$  since the resonant production is absent, bremsstrahlung is the dominant production mode,

$$\left. \frac{d\Gamma_L^{prod,V}}{d\omega dV} \right|_{brem} = \sum_{i=e,H,He} \epsilon_{T,L}^2 \frac{8Z_i^2 \alpha^3 n_e n_i m_V^2 \sqrt{\omega^2 - m_{A'}^2}}{3m_e^2 \omega^4} \sqrt{\frac{8m_e}{\pi T}} f\left(\sqrt{\frac{\omega}{T}}\right) \quad (B.7)$$

where

$$f(a) = \int_a^\infty dx x e^{-x^2} \log\left(\frac{x + \sqrt{x^2 - a^2}}{x - \sqrt{x^2 - a^2}}\right). \quad (B.8)$$

For H and He, we take the solar data from [87]. Note that there is a suppression of  $\alpha^3$  and thermal distribution ( $e^{-\omega/T}$ ) to the bremsstrahlung production mode for  $\omega > 300$  eV.

## References

- [1] P. Cushman et al., in *Community Summer Study 2013: Snowmass on the Mississippi (CSS2013) Minneapolis, MN, USA, July 29-August 6, 2013* (2013), [1310.8327](#), URL <http://arxiv.org/pdf/1310.8327.pdf>.
- [2] M. Pospelov, A. Ritz, and M. B. Voloshin, Phys.Rev. **D78**, 115012 (2008), [0807.3279](#).
- [3] J. Jaeckel and A. Ringwald, Phys. Lett. **B659**, 509 (2008), [0707.2063](#).
- [4] M. Ahlers, H. Gies, J. Jaeckel, J. Redondo, and A. Ringwald, Phys. Rev. **D76**, 115005 (2007), [0706.2836](#).
- [5] A. Wagner et al. (ADMX), Phys. Rev. Lett. **105**, 171801 (2010), [1007.3766](#).
- [6] R. Povey, J. Hartnett, and M. Tobar, Phys. Rev. **D82**, 052003 (2010), [1003.0964](#).
- [7] D. Horns, J. Jaeckel, A. Lindner, A. Lobanov, J. Redondo, and A. Ringwald, JCAP **1304**, 016 (2013), [1212.2970](#).
- [8] S. R. Parker, G. Rybka, and M. E. Tobar, Phys. Rev. **D87**, 115008 (2013), [1304.6866](#).
- [9] M. Betz, F. Caspers, M. Gasior, M. Thumm, and S. W. Rieger, Phys. Rev. **D88**, 075014 (2013), [1310.8098](#).
- [10] B. Döbrich, K. Daumiller, R. Engel, M. Kowalski, A. Lindner, et al. (2014), [1410.0200](#).
- [11] S. Chaudhuri, P. W. Graham, K. Irwin, J. Mardon, S. Rajendran, and Y. Zhao, Phys. Rev. **D92**, 075012 (2015), [1411.7382](#).
- [12] P. W. Graham, J. Mardon, S. Rajendran, and Y. Zhao, Phys. Rev. **D90**, 075017 (2014), [1407.4806](#).
- [13] C. Kouvaris and J. Pradler, Phys. Rev. Lett. **118**, 031803 (2017), [1607.01789](#).
- [14] S. Weinberg, Phys. Rev. Lett. **40**, 223 (1978).
- [15] F. Wilczek, Phys. Rev. Lett. **40**, 279 (1978).
- [16] R. D. Peccei and H. R. Quinn, Phys. Rev. Lett. **38**, 1440 (1977).
- [17] S. Dimopoulos, G. D. Starkman, and B. W. Lynn, Phys. Lett. **B168**, 145 (1986).
- [18] F. T. Avignone, III, R. L. Brodzinski, S. Dimopoulos, G. D. Starkman, A. K. Drukier, D. N. Spergel, G. Gelmini, and B. W. Lynn, Phys. Rev. **D35**, 2752 (1987).



- [19] C. E. Aalseth et al. (CoGeNT), Phys. Rev. Lett. **101**, 251301 (2008), [Erratum: Phys. Rev. Lett.102,109903(2009)], [0807.0879](#).
- [20] Z. Ahmed et al. (CDMS), Phys. Rev. Lett. **103**, 141802 (2009), [0902.4693](#).
- [21] E. Armengaud et al., JCAP **1311**, 067 (2013), [1307.1488](#).
- [22] E. Aprile et al. (XENON100), Phys. Rev. **D90**, 062009 (2014), [1404.1455](#).
- [23] Y. S. Yoon et al. (KIMS), JHEP **06**, 011 (2016), [1604.01825](#).
- [24] B. Holdom, Phys. Lett. **B166**, 196 (1986).
- [25] P. Galison and A. Manohar, Phys.Lett. **B136**, 279 (1984).
- [26] N. Arkani-Hamed, D. P. Finkbeiner, T. R. Slatyer, and N. Weiner, Phys.Rev. **D79**, 015014 (2009), [0810.0713](#).
- [27] M. Pospelov, A. Ritz, and M. B. Voloshin, Phys.Lett. **B662**, 53 (2008), [0711.4866](#).
- [28] M. Pospelov and A. Ritz, Phys. Lett. **B671**, 391 (2009).
- [29] J. Jaeckel and A. Ringwald, Ann.Rev.Nucl.Part.Sci. **60**, 405 (2010), [1002.0329](#).
- [30] J. Hewett, H. Weerts, R. Brock, J. Butler, B. Casey, et al. (2012), [1205.2671](#).
- [31] R. Essig, J. A. Jaros, W. Wester, P. H. Adrian, S. Andreas, et al. (2013), [1311.0029](#).
- [32] A. E. Nelson and J. Scholtz, Phys. Rev. **D84**, 103501 (2011), [1105.2812](#).
- [33] P. Arias, D. Cadamuro, M. Goodsell, J. Jaeckel, J. Redondo, and A. Ringwald, JCAP **1206**, 013 (2012), [1201.5902](#).
- [34] P. W. Graham, J. Mardon, and S. Rajendran, Phys. Rev. **D93**, 103520 (2016), [1504.02102](#).
- [35] H. An, M. Pospelov, J. Pradler, and A. Ritz, Phys. Lett. **B747**, 331 (2015), [1412.8378](#).
- [36] R. Essig, J. Mardon, and T. Volansky, Phys. Rev. **D85**, 076007 (2012), [1108.5383](#).
- [37] J. Angle et al. (XENON10), Phys. Rev. Lett. **107**, 051301 (2011), [Erratum: Phys. Rev. Lett.110,249901(2013)], [1104.3088](#).
- [38] R. Essig, A. Manalaysay, J. Mardon, P. Sorensen, and T. Volansky, Phys. Rev. Lett. **109**, 021301 (2012), [1206.2644](#).
- [39] E. Aprile et al. (XENON100) (2016), [1605.06262](#).
- [40] R. Agnese et al. (SuperCDMS), Phys. Rev. Lett. **116**, 071301 (2016), [1509.02448](#).
- [41] G. Fernandez Moroni, J. Estrada, G. Canelo, S. E. Holland, E. E. Paolini, and H. T. Diehl, Exper. Astron. **34**, 43 (2012), [1106.1839](#).
- [42] A. Aguilar-Arevalo et al. (2016), [1607.07410](#).
- [43] R. Essig, M. Fernandez-Serra, J. Mardon, A. Soto, T. Volansky, and T.-T. Yu, JHEP **05**, 046 (2016), [1509.01598](#).
- [44] P. W. Graham, D. E. Kaplan, S. Rajendran, and M. T. Walters, Phys. Dark Univ. **1**, 32 (2012), [1203.2531](#).
- [45] S. K. Lee, M. Lisanti, S. Mishra-Sharma, and B. R. Safdi, Phys. Rev. **D92**, 083517 (2015), [1508.07361](#).
- [46] Y. Hochberg, Y. Kahn, M. Lisanti, C. G. Tully, and K. M. Zurek (2016), [1606.08849](#).
- [47] S. Derenzo, R. Essig, A. Massari, A. Soto, and T.-T. Yu (2016), [1607.01009](#).

- [48] Y. Hochberg, M. Pyle, Y. Zhao, and K. M. Zurek, JHEP **08**, 057 (2016), [1512.04533](#).
- [49] Y. Hochberg, Y. Zhao, and K. M. Zurek, Phys. Rev. Lett. **116**, 011301 (2016), [1504.07237](#).
- [50] Y. Hochberg, T. Lin, and K. M. Zurek, Phys. Rev. **D94**, 015019 (2016), [1604.06800](#).
- [51] R. Essig, J. Mardon, O. Slone, and T. Volansky (2016), [1608.02940](#).
- [52] R. Budnik, O. Chechnovsky, O. Slone, and T. Volansky (to appear).
- [53] K. Schutz and K. M. Zurek, Phys. Rev. Lett. **117**, 121302 (2016), [1604.08206](#).
- [54] A. Derevianko, V. Dzuba, V. Flambaum, and M. Pospelov, Phys.Rev. **D82**, 065006 (2010), [1007.1833](#).
- [55] B. Henke, E. Gullikson, and J. Davis, Atom.Data Nucl.Data Tabl. **54**, 181 (1993).
- [56] *X-ray interactions with matter*, [http://henke.lbl.gov/optical\\_constants/](http://henke.lbl.gov/optical_constants/), accessed: 2016-08-04.
- [57] E. D. PALIK, in *Handbook of Optical Constants of Solids*, edited by E. D. PALIK (Academic Press, Boston, 1985), pp. 429 – 443, ISBN 978-0-08-054721-3, URL <http://www.sciencedirect.com/science/article/pii/B9780080547213500204>.
- [58] R. F. POTTER, in *Handbook of Optical Constants of Solids*, edited by E. D. PALIK (Academic Press, Boston, 1985), pp. 465 – 478, ISBN 978-0-08-054721-3, URL <http://www.sciencedirect.com/science/article/pii/B9780080547213500228>.
- [59] D. F. EDWARDS, in *Handbook of Optical Constants of Solids*, edited by E. D. PALIK (Academic Press, Boston, 1985), pp. 547 – 569, ISBN 978-0-08-054721-3, URL <http://www.sciencedirect.com/science/article/pii/B9780080547213500290>.
- [60] J. E. ELDRIDGE, in *Handbook of Optical Constants of Solids*, edited by E. D. PALIK (Academic Press, Boston, 1985), pp. 853 – 874, ISBN 978-0-08-054721-3.
- [61] E. Saloman and J. Hubbel (1986).
- [62] P. Sikivie, Lect. Notes Phys. **741**, 19 (2008), [19(2006)], [astro-ph/0610440](#).
- [63] D. J. E. Marsh, Phys. Rept. **643**, 1 (2016), [1510.07633](#).
- [64] J. Redondo, JCAP **1312**, 008 (2013), [1310.0823](#).
- [65] F. T. Avignone, III, R. J. Creswick, and S. Nussinov, Phys. Lett. **B681**, 122 (2009), [0903.4451](#).
- [66] H. An, M. Pospelov, and J. Pradler, Phys. Rev. Lett. **111**, 041302 (2013), [1304.3461](#).
- [67] J. Redondo, JCAP **0807**, 008 (2008), [0801.1527](#).
- [68] H. An, M. Pospelov, and J. Pradler, Phys. Lett. **B725**, 190 (2013), [1302.3884](#).
- [69] R. Essig, T. Volansky, and T.-T. Yu (2017), [1703.00910](#).
- [70] S. Golwala (SuperCDMS), *SuperCDMS SNOLAB: Goals, Design, and Status* (2016), talk given at UCLA DM 2016, URL <https://conferences.pa.ucla.edu/dm16/talks/golwala.pdf>.
- [71] A. Aguilar-Arevalo et al. (DAMIC), Submitted to: Phys. Rev. Lett. (2016), [1611.03066](#).
- [72] B. G. Lowe, Nuclear Instruments and Methods in Physics Research A **399**, 354 (1997).
- [73] M. Lépy, J. Campbell, J. Laborie, J. Plagnard, P. Stemmler, and W. Teesdale, Nuclear Instruments and Methods in Physics Research Section A: Accelerators, Spectrometers,

- Detectors and Associated Equipment **439**, 239 (2000), ISSN 0168-9002, URL <http://www.sciencedirect.com/science/article/pii/S0168900299009328>.
- [74] B. G. S. B. Streetman, Prentice Hall (2005).
  - [75] C. A. Klein, Journal of Applied Physics **39**, 2029 (1968).
  - [76] A. Robinson (SuperCDMS), *Controlling cosmogenic radioactivity in SuperCDMS SNOLAB* (2016), talk given at APS April Meeting 2016, URL <http://meetings.aps.org/Meeting/APR16/Session/M16.7>.
  - [77] J. Barreto et al. (DAMIC Collaboration), Phys.Lett. **B711**, 264 (2012), [1105.5191](#).
  - [78] J. Estrada and J. Tiffenberg (private communication).
  - [79] K. A. Olive et al. (Particle Data Group), Chin. Phys. **C38**, 090001 (2014).
  - [80] G. G. Raffelt, Phys. Lett. **B166**, 402 (1986).
  - [81] J. Redondo and G. Raffelt, JCAP **1308**, 034 (2013), [1305.2920](#).
  - [82] S. I. Blinnikov and N. V. Dunina-Barkovskaya, Mon. Not. Roy. Astron. Soc. **266**, 289 (1994).
  - [83] M. M. Miller Bertolami, B. E. Melendez, L. G. Althaus, and J. Isern, JCAP **1410**, 069 (2014), [1406.7712](#).
  - [84] J. Isern, E. Garcia-Berro, S. Torres, and S. Catalan, Astrophys. J. **682**, L109 (2008), [0806.2807](#).
  - [85] J. Isern, S. Catalan, E. Garcia-Berro, and S. Torres, J. Phys. Conf. Ser. **172**, 012005 (2009), [0812.3043](#).
  - [86] Y. Hochberg, T. Lin, and K. M. Zurek, Phys. Rev. **D95**, 023013 (2017), [1608.01994](#).
  - [87] C. Pena-Garay and A. Serenelli (2008), [0811.2424](#).